Design of the Precisely Tunable Central Frequency in BPF for Infrared Receiver

Lei Tian Member IAENG, Qinqin Li, Zhong Chen, Shujuan Chang, Weiheng Wang

***Abstract*—With the principle of the traditional band pass filter (BPF) and the 0.6-μm BiCMOS process, an operational transconductance amplifier (OTA-C) type BPF which central frequency could be tuned linearly in the infrared receiver (IR) chip was proposed. The BPF uses the improved bipolar OTA circuit. The pre-stage of the negative feedback increases the input voltage range. The second stage is the differential transconductance amplifier which tunes the central frequency linearly. The whole circuit is simulated by the Cadence software. When the working temperature is 25℃ and the working voltage is 5V, the result shows that central frequency could quadrature tunable and the central frequency could be linear adjusted between 24 KHz and 49 KHz. The central frequency is 35.04 KHz and the gain is 21.45dB while the frequency modulation (FM) code is 10010. The test results can satisfy the actual needs in the IR chip.**

***Index Terms*—Linearly adjustable, band pass filter, operational transconductance amplifier, central frequency**

I. Introduction

The infrared wireless communication is the point to point data transmission technology. Generally, its communication distance is short and the transmission rate is fast [1, 2]. The communication carrier uses the near infrared signal. It is widely used in the household appliance, car audio and the navigation system with its low cost and high transmission speed.

The infrared communication system is divided into three parts: the transmit module, the transmission medium and the receive module. In the transmit module, the user can generate different binary signals with various keys in the keyboard. Then the encoding circuit codes the binary signals and converts them into the transmission data. In the transmission part, the FM circuit modulates the encoded data with a pulse carrier and finally drives the IR light emitting diode to send the data [3,4].

The receive module mainly includes the photodiode (PD), the demodulation circuit and the microprocessor. The PD detects the infrared signal and converts it into an electrical signal. Finally, the microprocessor decodes the signal and control the device.

The infrared receiver is the most important part in the infrared communication system, the better performance of the infrared receiver circuit is required in the application [5]. After the transmission in the air, the infrared signal becomes very weak at the receiver. So, the infrared receiver chip is easily disturbed by the ambient light. Therefore, how to restrain the ambient interferences and improve the sensitivity of the infrared receiver is very important [6-8]. In this paper, the central frequency linear adjustable OTA-C band pass filter for infrared receiver is presented.

In the receive module, it got the modulated signal with different carrier frequency, so the carrier signal needs to be demodulated at the corresponding frequency. The traditional filter uses the analogue switch to regulate the central frequency [9-11]. But the switch range is limited and it could not meet the dynamic tune requirements.

The OTA-C type band pass filter (BPF) consists of the operational transconductance amplifier (OTA) and the capacitors (C). The important parameters about BPF are analyzed in detailed at first. Based on the principle of the OTA, designed an OTA-C type BPF with the central frequency and the Q-factor quadrature modulated [12-14]. It could adjust the central frequency within 27 KHz~48 KHz and prevent the interference from the ambient light.

II. Basic principle of the BPF

A. Circuit structure

The LC ladder BPF has the advantages of high reliability and sensitivity, but its central frequency and Q-factor cannot be quadrature modulated. So, it can't be used in the IR chip. Therefore, a narrowband filter is required, which can weaken various noises in the environment or internal circuits. In order to achieve the central frequency modulated, the narrowband BPF was constructed [15]. The circuit of the BPF is mainly consists of the two OTA, the resistors and the capacitors [16, 17], the circuit is shown in Fig. 1.

B. Circuit principle

The system function of the BPF is:

Manuscript received Nov 21, 2022; revised Feb 28, 2023.

This work was supported in the Natural Science Basic Research Program of Shaanxi (No. 2021JM-460), the Scientific Research Program of Shaanxi Provincial Education Department (No. 21JC033) and the Science and Technology Project of Xi'an city. (No. 22GXFW0126).

Lei Tian is a vice professor of the School of Electronic Engineering, Xi'an University of Posts and Telecommunications, Xi'an 710121 China. (phone: 086-029-88166-264; fax: 086-029-88166-273; e-mail: tianlei@xupt.edu.cn).

Qinqin Li is a PhD candidate of the Department of Electronic Engineering, Xi'an University of Posts and Telecommunications, Xi'an 710121 China. (e-mail: ttla02@163.com).

Zhong Chen is a professor of the Department of Electrical Engineering, University of Arkansas, Arkansas, 72201, USA (e-mail: tla02@126.com).

Shujuan Chang is a teacher of School of Electronic Engineering, Xi'an University of Posts and Telecommunications, Xi'an 710121 China. (e-mail: tlnwu@nwu.edu.cn).

Weiheng Wang is an engineer of the Institution Sup Galilée, Université Paris 13, Villetaneuse, Paris, 75001, France (e-mail: wxh2324@ 126.com).

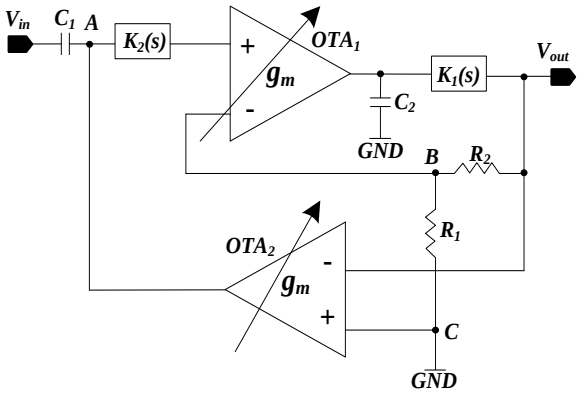

Fig. 1. The circuit of the second-level BPF

$$H(s)=\frac{H_0\frac{\omega_0}{Q}s}{s^2+\frac{\omega_0}{Q}s+\omega_0^2} \tag{1}$$

Here, H_0 is the gain of BPF, ω_0 is the central frequency, Q is the quality factor. The BPF is constructed by the low-pass filter and the high-pass filter. The low-pass filter is C_2 and OTA_2. The high-pass filter is C_1, OTA_1, R_1 and R_2. g_m is the gain of OTA. The frequency selective network $K(s)$ controls the tail current to change the g_m [18, 19]. Thus the center frequency could be adjustable. The output voltage (V_o), the output current (I_o), the input voltage (V_i) and its input current (I_i) of the network $K_1(s)$ are showned as below:

$$K_V(s)=\frac{V_o(s)}{V_i(s)}=1 \tag{2}$$

$$K_I(s)=\frac{I_o(s)}{I_i(s)}=K_1 \tag{3}$$

At the point of A, B and C, three equations can be listed:

$$\begin{cases} sC_1(V_{IN}-V_A)=g_mV_{OUT} \\ \frac{V_B}{R_1}=\frac{V_{OUT}}{R_1+R_2} \\ g_m(V_A-V_B)=sC_2V_{OUT}+\frac{V_{OUT}}{K_1(R_1+R_2)} \end{cases} \tag{4}$$

The system function of BPF is:

$$H(s)=\frac{V_{OUT}}{V_{IN}}=\frac{\frac{g_m}{C_2}s}{s^2+s\frac{g_mR_1+1/K_1}{C_2(R_1+R_2)}+\frac{g_m^2}{C_1C_2}} \tag{5}$$

Where $g_mR_1>>1/K$, comparing Equation (5) with Equation (1), w_0, Q and H (0) can be calculated by the following:

$$\begin{cases} \omega_0=\frac{g_m}{\sqrt{C_1C_2}} \\ Q=(1+\frac{R_2}{R_1})\sqrt{\frac{C_2}{C_1}} \\ H(0)=1+\frac{R_2}{R_1} \end{cases} \tag{6}$$

İn equation (6), w_0 is the inversely proportional with C_1C_2. After fixed the value of C_1 and C_2, through changing the value of g_m, R_1 and R_2, the w_0 and Q can be quadrature. If the g_m can be adjusted, the w_0 can be tuned linearly.

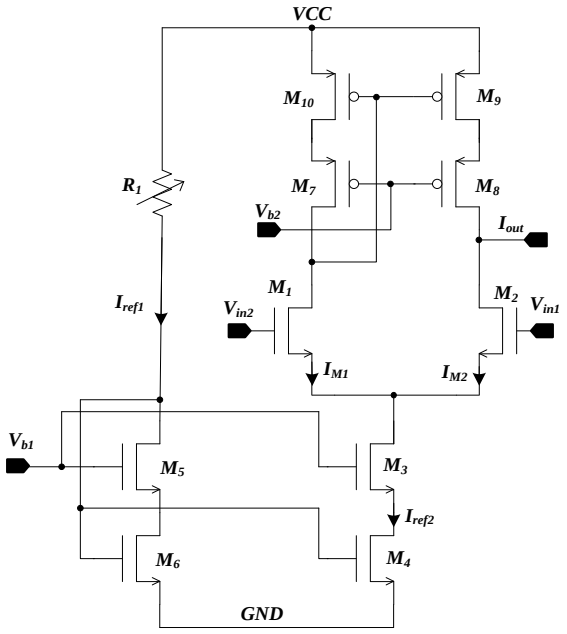

Fig. 2. The traditional CMOS type OTA circuit

III. Proposed OTA circuit

A. Traditional circuit structure

The conventional metal oxide semiconductor (MOS) type OTA uses the basic differential pairs to construct the circuit [20, 21]. To achieve the precise current, the Cascode current mirror is used as the current source and the load [22]. The circuit is shown in Fig. 2.

Assume the transistor working in the saturated state, the output current is:

$$I_{out}=I_{M_1}-I_{M_2}=g_m(V_{in1}-V_{in2}) \tag{7}$$

It can be seen from equation (7) that the dynamic input range is small, so it doesn't suitable for the narrowband filter in the IR chip.

B. Improved OTA circuit structure

The improved OTA circuit was constructed by the

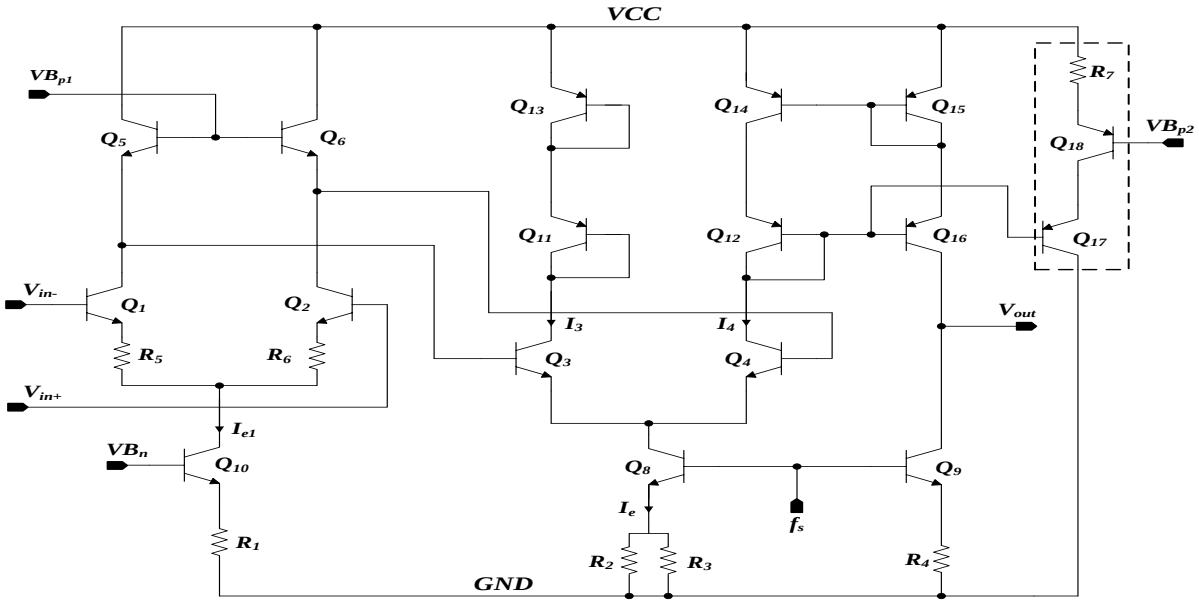

Fig. 3. The improved OTA circuits

two-level differential structures as shown in Fig. 3.

The amplifier has a two-stage differential structure. The first stage uses the emitter negative feedback to reduce the input voltage. The second stage is the differential transconductance amplifier. In the output stage, R_7, Q_{17} and Q_{18} construct the Wilson current source.

In the first stage, the voltage reduction ratio can be adjusted by the value of R_5 and R_6. It ensures the accurate g_m of the second-stage transconductance amplifier. With the input voltage increasing, the differential input signal in the second stage was reduced. The ration of the tail current through the Q_8 and Q_9 is 2:1 for case where R_2=R_3=R_4. Then the gain of the output can be confirmed where R_5 = R_6. In the output stage, the Wilson current source increases the output resistance and guarantees the accuracy of the output current.

C. Analyze the circuit principle

In Fig.3, the OTA's g_m is proportional to the central frequency of the BPF, with the large signal method, the value of g_m is calculated at first.

I_{e1} is the current through Q_{10}, ΔI_{e1} is the current difference between Q_1 and Q_2. The gain of the circuit is A_1 and calculated as below:

$$\Delta V_{in} = R_5 \Delta I_e + V_t \ln[(\frac{1}{2} I_e + \frac{1}{2}\Delta I_e)/(\frac{1}{2} I_e - \frac{1}{2}\Delta I_e)] \quad (8)$$

$$\Delta V_{out} = V_t \ln[(\frac{1}{2} I_e + \frac{1}{2}\Delta I_e)/(\frac{1}{2} I_e - \frac{1}{2}\Delta I_e)] \quad (9)$$

$$A_1 = \frac{V_t \ln \frac{I_e + \Delta I_e}{I_e - \Delta I_e}}{R_5 \Delta I_e + V_t \ln \frac{I_e + \Delta I_e}{I_e - \Delta I_e}} \quad (10)$$

From equation (10), if R_5 is large enough and $A_1 << 1$, the g_m of OTA can be written as:

$$g_m = A_1 \times g_{m2} \quad (11)$$

Here, g_{m2} is the second stage gain. In order to get g_m, g_{m2} should be calculated firstly. In Figure 3, I_e is the tail current through Q_8, I_3 and I_4 are the current through Q_3 and Q_4, respectively. It can be expressed as:

$$I_3 = \frac{I_e}{1 + e^{\frac{V_{BE4} - V_{BE3}}{V_T}}} \quad (12)$$

Assume $\frac{V_{BE2} - V_{BE1}}{2V_T} = x$:

$$I_3 = \frac{I_e}{1 + e^{2x}} = \frac{I_e}{2}[1 - \tanh(x)] \quad (13)$$

Then I_4 and I_{out} can be achieved:

$$I_4 = \frac{I_e}{2}[1 + \tanh(x)] \quad (14)$$

$$I_{out} = \frac{1}{2}(I_3 - I_4) = -\frac{1}{2} I_e \tanh(\frac{\Delta V_{BE}}{2V_T}) \quad (15)$$

Then g_{m2} can be calculated:

$$g_{m2} = \frac{\partial I_{out}}{\Delta V_{BE}} = -\frac{I_e}{4V_T}[1 - \tanh^2(\frac{\Delta V_{BE}}{2V_T})] \quad (16)$$

From equation (11) and equation (16), the g_m of the circuit is:

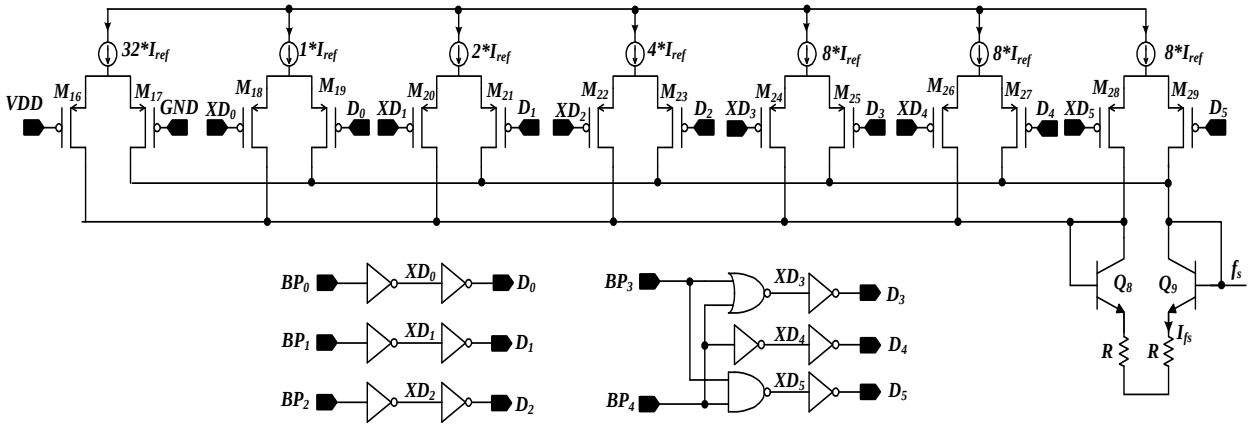

Fig. 4. Frequency Modulation circuit

$$g_m = \frac{V_t \ln[(\frac{1}{2}I_e + \frac{1}{2}\Delta I_e)/(\frac{1}{2}I_e - \frac{1}{2}\Delta I_e)]}{R_5 \times \Delta I_e + V_t \ln[(\frac{1}{2}I_e + \frac{1}{2}\Delta I_e)/(\frac{1}{2}I_e - \frac{1}{2}\Delta I_e)]} \times \frac{-I_e}{4V_T}[1-\tanh^2(\frac{\Delta V_{BE}}{2V_T})] \quad (17)$$

In the IR receiver, the pre-stage circuit of the BPF is always the variable gain amplifier. The input signal of BPF would be hundreds or even thousands of millivolt. Therefore, the voltage gain of the first stage can be get by adjusting the R_5 and R_6. So the amplitude of the input signal in the second stage is within the linear range. We can change the value of tail current through Q_8 to adjust g_m. At the same time, as long as I_e can be linear adjusted, the central frequency linear tunable will be achieved.

IV. Design the FM circuit

To save the chip area and reduce the power consumption, the FM circuit is constructed with the CMOS process. In the IR communication, the range of the carrier frequency between 33 KHz and 40 KHz. Considering the process deviation, designed 20% margin and the range of the modulation is from 26 KHz to 48 KHz.

The traditional FM circuit can be achieved by adjusting the resistance in the bias circuit. This method is easy to implement and simple to operate. However, with the temperature characteristics of the device and the process deviation, the circuit will occur more error. In order to overcome the above issues, this paper uses the FM circuit to modulate the mirror current I_e. The complete schematic of the FM circuit is shown in Fig. 4.

The current I_{fs} flows through Q_9 is consisted of seven branches current. The left branch is the bias current which value is $32I_{ref}$ and the other branches are controlled by the signal D_0~D_5. When these signals are low level, the branch current flows through Q_9, otherwise through Q_8. So the current through Q_9 is:

$$\begin{aligned} I_{fs} &= 32I_{ref} + I_{ref}(\overline{D_0} + 2\overline{D_1} + 4\overline{D_2} + 8\overline{D_3} + 8\overline{D_4} + 8\overline{D_5}) \\ &= 32I_{ref} + I_{ref}(2^0\overline{BP_0} + 2^1\overline{BP_1} + 2^2\overline{BP_2} + 2^3\overline{BP_3} + 2^4\overline{BP_4}) \end{aligned} \quad (18)$$

From equation (18), the seven branches current have 2^5 combination, the range of I_{fs} from $32I_{ref}$ to $[32+(2^5-1)]*I_{ref}$. Here, set $Q=BP_4BP_3BP_2BP_1BP_0$, the equation (18) can be simplified as:

$$I_{fs} = 32I_{ref} + I_{ref}Q \quad (19)$$

At the same time, the existence of the branch Q_8 provides a symmetrical relationship for Q_9. Whether D_0~D_5 are low or high, this structure makes the seven branches current flow through this path. It reduces the variation of the current from the power supply to the ground and the noise of the power.

From Eq (17), I_{fs} can be linear modulated. For the mirror relationship between I_e and I_{fs}, I_e also can be adjusted. So the central frequency of the BPF can be tuned linearly.

V. Simulation and Test Result

A. Simulation result

In this section, the BPF with the central frequency linear tunable was presented in the IR receiver. At the same time, we designed the FM circuit to adjust the central frequency. The chip is fabricated by the 0.6 μm BiCMOS process. Its area is 1.2*0.6 mm^2. The photograph is showed in Fig. 5(a). The V_{bias} module is the power supply for the photoelectronic process circuit. The PD converts the incites photons into photocurrent. The photocurrent is converted into voltage signal through the TIA. The BPF and the FM module are the bandpass filter circuit and the frequency modulation circuit which were explained in details in the above section. The layout of the chip is showed in Fig. 5 (b), the device layout and signal direction correspond to Fig. 5(a).

In order to test the relationship with the FM code, the bias current and the central frequency is simulated by the Cadence software with the 0.6 μm BiCMOS technology. In the typical condition, when the working temperature is 25℃ and the VCC is 5V, the simulation data are showed in Table 1 and the results are showed in Fig. 6.

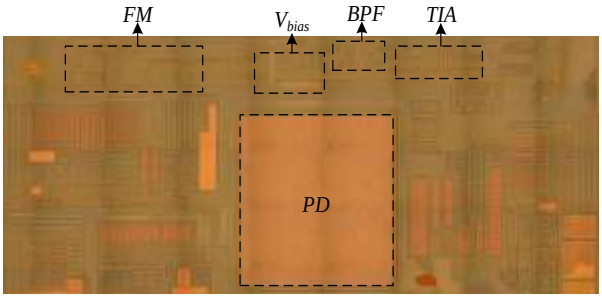

(a) The chip photograph

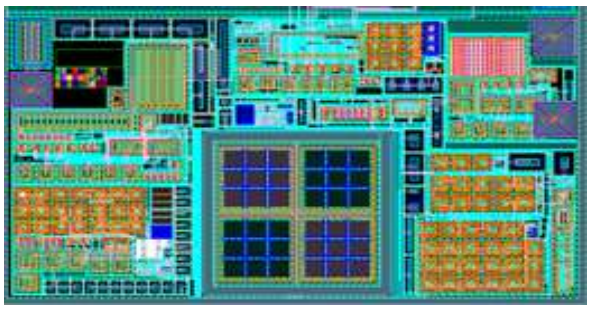

(b)The chip layout

Fig. 5. The photograph and the layout

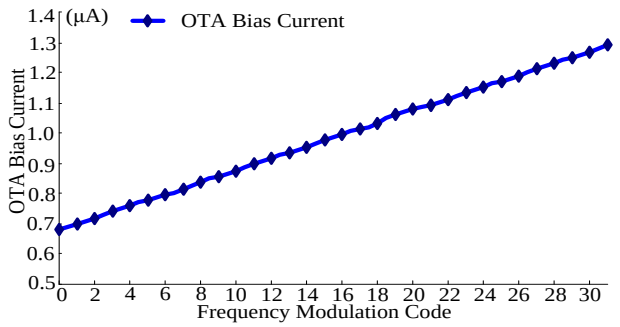

(a)FM code and the OTA bias current

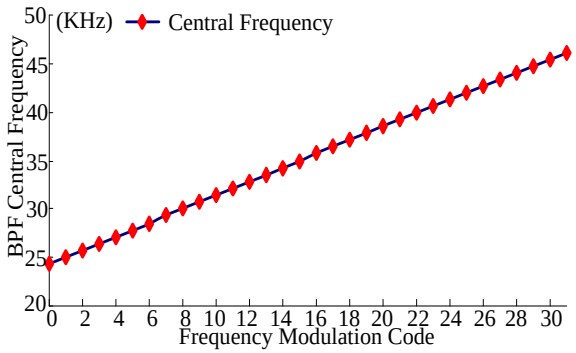

(b) FM code and the BPF central frequency

Assuming the process drift is 20%, Fig. 6(a) shows the relationship between the FM code and the OTA bias current. The simulation results show the FM code and the OTA bias current have a stable linear relationship. When the FM code is determined, the OTA bias current value is stable. Under the same FM coding conditions, the FM code also has the linear relationship with the BPF central frequency in Fig. 6(b). The

TABLE I
SIMULATION DATA

FM code	Central Frequency (KHz)	OTA Bias current (uA)	Error Ratio	Gain （dB）
0	24.95	1.008	0.92%	19.82
1	25.41	1.025	0.80%	19.83
2	25.76	1.042	0.81%	19.87
3	26.24	1.059	0.87%	19.88
4	26.67	1.078	0.86%	19.90
5	27.16	1.097	0.87%	19.92
6	27.61	1.117	0.92%	19.95
7	28.18	1.137	0.91%	19.95
8	28.64	1.158	0.86%	19.98
9	29.17	1.18	0.98%	20.00
10	29.78	1.204	0.98%	20.02
11	30.34	1.227	0.98%	20.04
12	30.97	1.252	1.03%	20.06
13	31.62	1.278	1.10%	20.08
14	32.36	1.305	1.10%	20.10
15	33.04	1.333	0.98%	20.12
16	33.65	1.363	1.15%	20.13
17	34.59	1.393	1.21%	20.16
18	35.32	1.426	1.10%	20.19
19	36.14	1.46	1.21%	20.21
20	37.06	1.495	1.22%	20.24
21	37.95	1.532	1.27%	20.26
22	38.99	1.572	1.31%	20.28
23	39.99	1.613	1.27%	20.31
24	41.02	1.657	1.33%	20.33
25	42.17	1.703	1.38%	20.36
26	43.35	1.752	1.50%	20.38
27	44.77	1.803	1.55%	20.41
28	46.13	1.858	1.44%	20.44
29	47.42	1.916	1.50%	20.46
30	48.98	1.979	1.73%	20.49

corresponding center frequency can be adjusted from 24KHz to 48KHz, which meets the requirements of infrared receiver.

İt can be can see from Table 1, with different FM code, the corresponding central frequency can become from 24.95KHz to 48.98KHz. The maximum error of the center frequency is 1.73%. The gain changed from 19.82dB to 20.49dB.

B. Test result

With the designed BPF structure, the IR has the good characteristic of the linear adjustment. The packaged chip photograph and our test platform are shown in Fig. 7.

Fig. 7(a) is the photo of the packaged chip, with the length of 5.0 mm. Fig. 7(b) is the actual test platform, including light source, reflector and chip bracket. In order to verify the performance of the BPF in the IR receiver, we selected 35KHz as the central frequency and test the IR chip with the oscilloscope SA1005A. When the input voltage is 5V, set 10010 as the modulation frequency code, the test result in frequency domain was showed in Figure 8.

The upper half of Fig. 8 is the simulation result of the BPF frequency response. The central frequency is 35.04 KHz. The bandwidth is 3.799 KHz and the gain is 21.45 dB. The bottom half of Figure 8 is the test result in the frequency

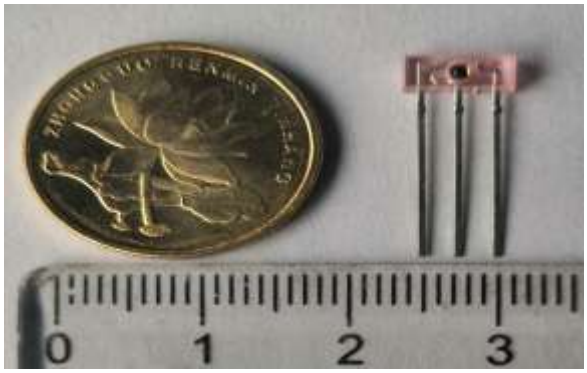

(a) Photograph of the packaged chip

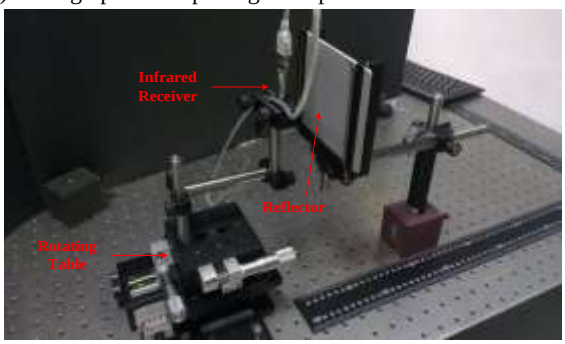

(b)The test platform

Fig. 7. The chip and the test platform

domain. Its central frequency is 35.04 KHz and the bandwidth is 3.8 KHz. Compared with the simulation result, it can be concluded that the test result match the simulation results very well. It is testified that the proposed BPF has a good filtering effect for a specific frequency, and its gain gradually increases with the center frequency increases.

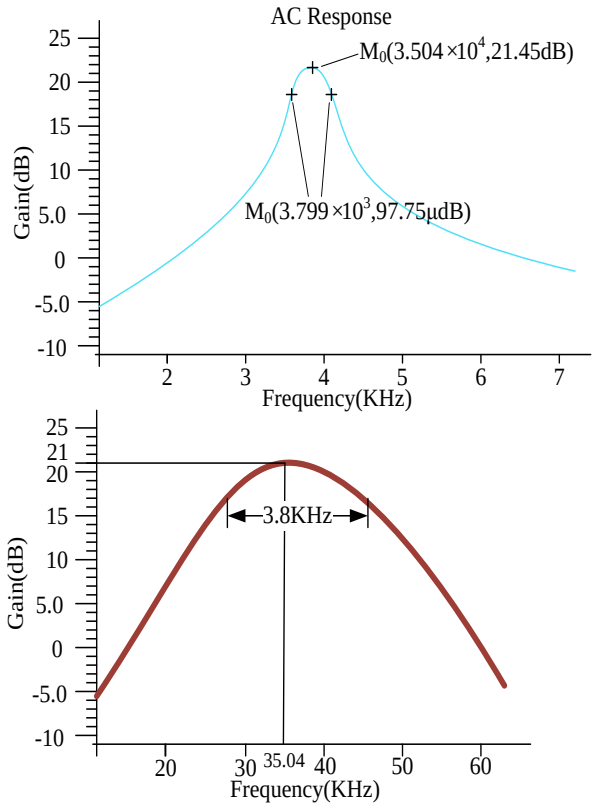

Fig. 8. Comparison of the simulation and test result

In order to show the effect of our design, the key parameters are compared in Table 2.

TABLE II
COMPARISON WITH OTHER REPORTED REFERENCES

	[1]	[2]	[3]	[4]	This work
Technology (μm)	0.18	0.18	0.18	0.18	0.6
Input Voltage	1.8V	60mV	1V	1V	5V
Bandwidth (Hz)	300-10K	0.6M	250	50	24-49K
Gain(dB)	52.5-57.5	0	61.2	49.9	19.82-20.49
Area(mm^2)	-	0.15	0.24	0.12	0.72

It can be seen from the comparison, the measured bandwidth nd gain of the BPF in this paper meet the simulation index. Within the bandwidth of 25KHz, the linearly adjustable area is 3.8KHz and the circuit maintains a high gain.

VI. CONCLUSION

In this work, compared with the conventional OTA circuit, the improved OTA structure is proposed. Then the FM circuit suitable for the infrared receiver circuit is designed. Based on the traditional BPF theory, a second stage BPF with the OTA-C structure is proposed. The simulation results show the FM code have stable linear relationship between the OTA bias current and the BPF central frequency. With the good linear characteristic, the OTA circuit can be adjusted from 24 KHz to 49 KHz. When the working voltage is 5 V and working temperature is 25 C°, the gain of the circuit is 21 dB. The central frequency can be adjusted linearly within the band of 3.8 KHz. The BPF meets the design specifications for the IR. The circuit can realize the linear adjustment of the center frequency. Its output is stable and it meets the actual requirements in the infrared communication process.

REFERENCES

[1] H. Rezaee-Dehsorkh, N. Ravanshad, R. Lotfi, K. Mafinezhad and A. M. Sodagar, "Analysis and Design of Tunable Amplifiers for Implantable Neural Recording Applications," *IEEE.J. Em. Sel. Top. C*, vol. 1, no. 4, pp. 546-556, 2011.

[2] A. Rasekh and M. Sharif Bakhtiar, "Design of Low-Power Low-Area Tunable Active RC Filters," *IEEE.T.Circuits*-II, vol. 65, no. 1, pp. 6-10, 2018.

[3] S. Lee, C. Wang and Y. Chu, "Low-Voltage OTA–C Filter With an Area- and Power-Efficient OTA for Biosignal Sensor Applications," *IEEE.T.Biomed.Circ.S*, vol. 13, no. 1, pp. 56-67, 2019.

[4] C. Y. Sun and S. Y. Lee, "Fifth-order butterworth OTA–C LPF with multiple-output differential-input OTA for ECG applications," *IEEE.T.Circuits-II*, vol. 65, no. 4, pp. 421–425, 2018.

[5] W. Hu, H. Cong, W. Huang, Y. Huang, L. J. Chen, A. L. Pan and C. L. Xue, "Germanium/perovskite heterostructure for high-performance and broadband photodetector from visible to infrared telecommunication band," *Light-Sci.Appl*, vol. 8, no. 106, pp. 1-10, 2019.

[6] F. E. Alsaadi, A. M. Alhartomi and M. H. Jaafar Elmirghani, "Fast and Efficient Adaptation Algorithms for Multi-gigabit Wireless Infrared Systems," *J.Light.Wave.Tech*, vol. 31, no. 23, pp. 3735-3751, 2013.

[7] Z. Zhang, Y. F. Li, K. Mouthaan and Y. Lian, "A Miniature Mode Reconfigurable Inductor less IR-UWB Transmitter-Receiver for Wireless Short-Range Communication and Vital-Sign Sensing," *IEEE.J. Em.Sel.Top.C*, vol. 8, no. 2, pp. 394-305, 2018.

[8] J. C. Tong, F. Suo, L. Qian and D. H. Zhang, "Asymmetric Split H-Shape Resonator Array for Enhancement of Midwave Infrared Photodetection," *IEEE.J.Quant.Electr,* vol. 55, no. 6, pp. 400406-1-6, 2019.
[9] J. Xu, Z. Y. Chen and Q. H. Cai, "Design of Miniaturized Dual-Band Low-Pass–Bandpass and Bandpass Filters," *IEEE.T.Comp.Pack.Man.,* vol. 8, no. 1, pp. 132-139, 2018.
[10] C. S. Chen, J. F. Wu and Yoshen Lin."Compact Single-pole-double-Throw Switchable Bandpass Filter Based on Multicoupled Line."*IEEE.Microw.Wirel.Co.,* vol. 24, no. 2, pp. 87-89, 2014.
[11] F. C. Chen, R. S. Li and J. P. Chen. "A Tunable Dual-Band Bandpass-to-Bandstop Filter Using p-i-n Diodes and Varactors." *IEEE.Microw.Wirel.Co,* vol. 28, no. 1, pp. 888-890, 2018.
[12] S. Y. Peng, Y. S. Lee, T. Wang, H. C. Huang, M. R. Lai, C. Lee and L. H. Liu, "A Power-Efficient Reconfigurable OTA-C Filter for Low-Frequency Biomedical Applications," *IEEE.T.Circuits-I,* vol. 65, no. 2, pp. 543-555, 2018.
[13] D. A. Ginés, J. M. Carrillo-Calleja, J. Illade-Quinteiro, M. V. Félix, J. Á. Díaz-Madrid, F. Fernández-Luque and J. Zapata-Pérez, "Low-frequency CMOS Bandpass Filter for PIR Sensors in Wireless Sensor Nodes," *IEEE.Sens.J.,* vol. 14, no. 11, pp. 4085-4094, 2014.
[14] Z. J. Zhang, J. Luo, M. W. Song and H. L. Yu, "Large-area, Broadband and High-efficiency Near-infrared Linear Polarization Manipulating Metasurface Fabricated by Quadrature Interference Lithography," *Appl.Phys.Lett.,* vol. 107, no. 24, pp. 1904-242103, 2015.
[15] J. Kapoor, G.R Mishra, A. Pathak and M. Rai, "Analysis of BSC and AWGN Channel Distortion Effect on Sound Signal in Active Noise Cancellation Application," *Engineering Lett.,* vol. 29, no. 3, pp. 926-930, 2021.
[16] J. Xiao, X. Su, H. Wang and J. Ma, "Compact microstrip balanced bandpass filter with adjustable transmission zeros," *Electron.Lett,* vol. 55, no. 4, pp. 212-214, 2019.
[17] R. Mehra, V. Kumar and A. Slam., "Reliable and Q-Enhanced Floating Active Inductors and Their Application in RF Bandpass Filters," *IEEE.Access.* Vol. 6, pp. 48181–48194, 2018.
[18] Z. C. Lin, P. I. Mak and R. P. Martins, "Analysis and Modeling of a Gain-Boosted N-Path Switched-Capacitor Bandpass Filter," *IEEE.T.Circuits-I,* vol. 61, no. 9, pp. 2560-2568, 2014.
[19] M. Naimul Hasan, S. Saeedi, Q. J. Gu, H. H. Sigmarsson and X. G. Liu, "Design Methodology of N-Path Filters With Adjustable Frequency, Bandwidth, and Filter Shape," *IEEE.T.Microw.Theory.,* vol. 66, no. 6, pp. 2775-2790, 2018.
[20] X. Zhao, H. J. Fang, T. Ling and J. Xu, "Transconductance Improvement Technique for Bulk-driven OTA in Nanometre CMOS Process," *Electro.Lett.,* vol. 51, no. 22, pp. 1758-1759, 2015.
[21] D. K. Du and K. M. Odame, "A Bandwidth-Adaptive Preamplifier," *IEEE.J.Solid-St.Circ.,* vol. 48, no. 9, pp. 2142-2153, 2013.
[22] O. Channumsin and W. Tangsrirat, "Electronically Tunable Floating Capacitance Multiplier Using FB-VDBAs," *Engineering Lett.,* vol. 24, no. 3, pp. 365-369, 2016.

Lei Tian received his master's degree in mobile communication from Xi'an University of Science and Technology in 2006. In 2015, he received his Ph.D. in optoelectronic integrated circuit design (OEIC) from Xidian University. In 2019, he completed his postdoctoral study in Northwest University. His research interests include analog and mixed integrated circuits, photoelectric signal processing, optocouplers, SOC design, and IR communications. (tianlei@xupt.edu.cn).

Qinqin Li received her master's degree in circuits and systems from Xidian University in 2014. Since then, she has been pursuing a doctoral degree from Xidian University. Her research interests include digital and analog mixed integrated circuits and optoelectric processing circuits.

Zhong Chen received his doctorate in electrical engineering from North Carolina State University, a master's degree in electrical engineering from National University of Singapore, and a bachelor's degree in instrumentation science and engineering from Zhejiang University, China. He worked for six and half years as an ESD specialist in the Analog Technology Development at Texas Instruments prior to joining the Faculty of Electrical Engineering, University of Arkansas in 2015 as an assistant professor.

Shu-juan Chang was born in Xi'an City, in 1980. She received the Master degree in Communication and information engineering in 2006. Then she has been working in Xi'an University of Posts & Telecommunications. Her research interest includes Image processing and pattern recognition, digital and analog circuits.

Weiheng Wang received his B.S. degree in electronics from Xi'an University of Posts and Telecommunications in 2010. He received his master's degree and engineer title in telecoms and networks from Institut Sup Galilée, Université Paris 13, Villetaneuse, France in 2014. Since 2014, he has been working for Vente-Privée (French's top e-commerce firm). His research interests include power electronics and the design and testing of integrated optoelectric circuits.